Title	Multi-channel pre-beamformed data acquisition system for research on advanced ultrasound imaging methods
Author(s)	Cheung, CCP; Yu, ACH; Salimi, N; Yiu, BYS; Tsang, IKH; Kerby, B; Azar, RZ; Dickie, K
Citation	IEEE Transactions On Ultrasonics, Ferroelectrics, And Frequency Control, 2012, v. 59 n. 2, p. 243-253
Issued Date	2012
URL	http://hdl.handle.net/10722/145559
Rights	IEEE Transactions on Ultrasonics, Ferroelectrics and Frequency Control. Copyright © IEEE

Multi-Channel Pre-Beamformed Data Acquisition System for Research on Advanced Ultrasound Imaging Methods

Chris C. P. Cheung, Alfred C. H. Yu, *Member, IEEE*, Nazila Salimi, Billy Y. S. Yiu, *Member, IEEE*, Ivan K. H. Tsang, Benjamin Kerby, Reza Zahiri Azar, *Member, IEEE*, and Kris Dickie

***Abstract*—The lack of open access to the pre-beamformed data of an ultrasound scanner has limited the research of novel imaging methods to a few privileged laboratories. To address this need, we have developed a pre-beamformed data acquisition (DAQ) system that can collect data over 128 array elements in parallel from the Ultrasonix series of research-purpose ultrasound scanners. Our DAQ system comprises three system-level blocks: 1) a connector board that interfaces with the array probe and the scanner through a probe connector port; 2) a main board that triggers DAQ and controls data transfer to a computer; and 3) four receiver boards that are each responsible for acquiring 32 channels of digitized raw data and storing them to the on-board memory. This system can acquire pre-beamformed data with 12-bit resolution when using a 40-MHz sampling rate. It houses a 16 GB RAM buffer that is sufficient to store 128 channels of pre-beamformed data for 8000 to 25 000 transmit firings, depending on imaging depth; corresponding to nearly a 2-s period in typical imaging setups. Following the acquisition, the data can be transferred through a USB 2.0 link to a computer for offline processing and analysis. To evaluate the feasibility of using the DAQ system for advanced imaging research, two proof-of-concept investigations have been conducted on beamforming and plane-wave B-flow imaging. Results show that adaptive beamforming algorithms such as the minimum variance approach can generate sharper images of a wire cross-section whose diameter is equal to the imaging wavelength (150 μm in our example). Also, plane-wave B-flow imaging can provide more consistent visualization of blood speckle movement given the higher temporal resolution of this imaging approach (2500 fps in our example).**

I. Introduction

Since its introduction in the latter half of the 20th century, ultrasound has emerged as a non-invasive imaging modality that can provide anatomical images in real time [1]. Over the years, a wide array of commercial ultrasound scanners has been made available on the market; these range from trolley-based systems that are intended for bedside applications to portable devices that suit point-of-care diagnoses. However, unlike other modalities such as magnetic resonance imaging, commercial ultrasound scanners are seldom reconfigurable because they are mostly developed via an embedded system design approach so that the hardware can fit within physical size constraints [2]. This design strategy inherently lacks flexibility in modifying front-end scanner operations, making it difficult for system researchers to carry out experimental investigations of new imaging schemes and algorithms because of the high cost and long time required to re-prototype scanners [3]. Indeed, many research efforts on ultrasound imaging methods have relied rather heavily on computational analyses that are insufficient on their own to characterize the performance of newly developed methods.

To enable experimental analysis of new ultrasound imaging methods, some groups have been devising research-purpose ultrasound imaging hardware that can acquire raw ultrasound data from a scanner's front-end [4]. The early versions of these have been developed in the form of add-ons that are designed specifically for clinical ultrasound scanners. For instance, research interfaces are now publicly available for the Siemens Antares scanner [5], Hitachi's HiVision scanner [6], and Zonare's z.one system [7]. In contrast, several academic laboratories have designed in-house systems for raw data acquisition [8]–[10]. There is also an attempt to develop an open-architecture scanner with raw data access, the Ultrasonix system [11], [12]. For these research interfaces or scanners, raw ultrasound data are considered to be the ones sampled after beamforming, which is an upstream processing step that influences the imaging resolution. Access to the post-beamforming ultrasound data (often called the RF data) is important for evaluation of new signal processing methods such as strain estimation [13] and adaptive color Doppler clutter filtering [14], [15]. However, it does not suffice for studies on next-generation imaging paradigms like transient elasticity imaging [16], synthetic aperture imaging [17], plane-wave compounding [18], high-frame-rate blood flow imaging [19], [20], adaptive beamforming [21], and photoacoustic imaging [22] that work with the pre-beamformed data of each element on the ultrasound array.

To more effectively foster research on advanced imaging paradigms, it is important to gain access to raw ultrasound data at the pre-beamformed level (sometimes called channel-domain data). In response to this research need, several pre-beamformed data acquisition tools have been developed. For instance, an add-on tool has been designed to acquire pre-beamformed data from a Philips Sonos-5500 scanner [23], and a similar feature has been implemented

Manuscript received July 26, 2011; accepted November 2, 2011.

C. C. P. Cheung, N. Salimi, B. Kerby, R. Zahiri Azar, and K. Dickie are with Ultrasonix Medical Corp., Richmond, BC, Canada (e-mail: kris.dickie@ultrasonix.com).

A. C. H. Yu, B. Y. S. Yiu, and I. K. H. Tsang are with the Medical Engineering Program, The University of Hong Kong, Pokfulam, Hong Kong SAR (e-mail: alfred.yu@hku.hk).

Digital Object Identifier 10.1109/TUFFC.2012.2184

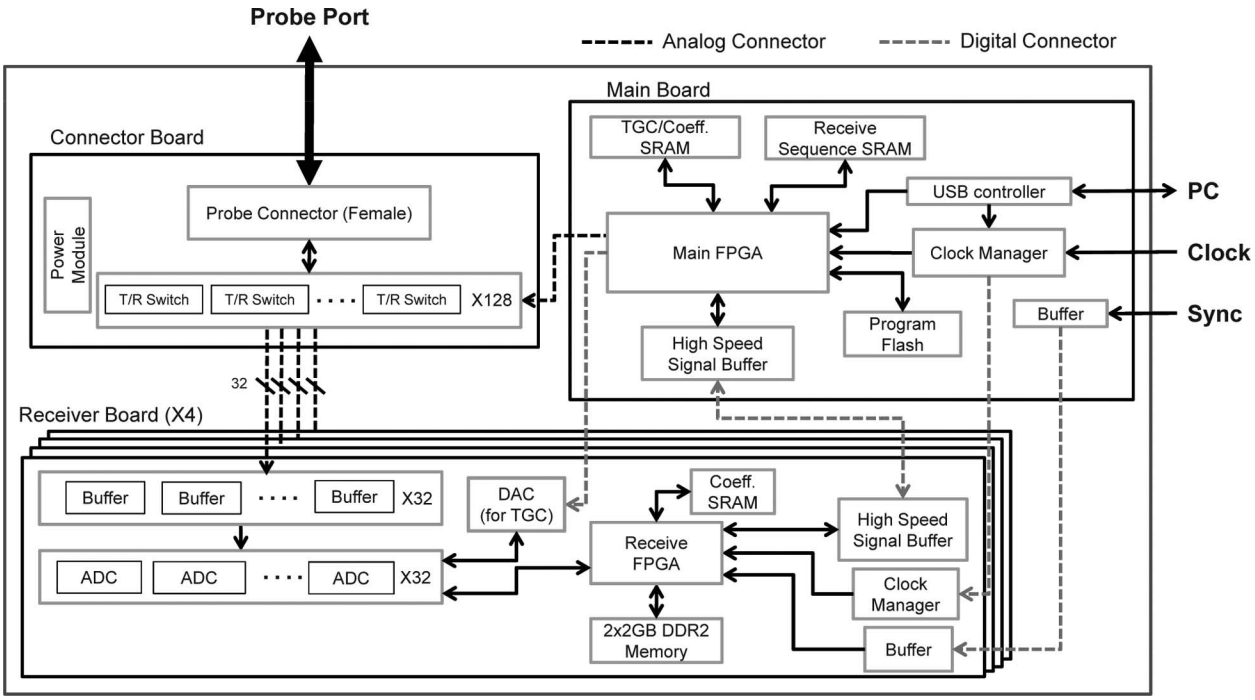

Fig. 1. Overall system architecture of the multi-channel pre-beamformed data acquisition system. This architecture has been designed to support parallel acquisition of pre-beamformed data in 128 channels from an array probe connected to an Ultrasonix scanner.

in the form of an extension to the Zonare z.one system [24]. A research platform with channel-domain processing capabilities has also been made commercially available by Verasonics [25]. In parallel to these efforts, a few academic laboratories have been developing their own customized systems with pre-beamformed data access [26]–[30].

In this paper, we present the development of a new pre-beamformed data acquisition (DAQ) system that can interface with the Ultrasonix series of open-architecture research scanners. Our developed system can acquire raw data from 128 transducer array elements in parallel, and it differs from many of the previously developed systems in that it is designed to work as a plug-and-play device without interrupting the scanner's normal operations during a diagnostic scan. In the subsequent sections, we shall describe the system's architecture and hardware components. Case examples will also be given to show how this system can be used in advanced ultrasound imaging research studies.

TABLE I. TECHNICAL SPECIFICATIONS OF THE PRE-BEAMFORMED DATA ACQUISITION SYSTEM.

Parameter	Value
Number of parallel receive channels	128
Sampling frequency	40 or 80 MHz
Sampling resolution	10 bits (for 80-MHz sampling) 12 bits (for 40-MHz sampling)
Amplifier gain	Up to 52 dB
Size of data storage memory	16 GB (DDR2)
Front-end connector link	Tyco 156-pin male head
Back-end data transfer link	USB 2.0
On-board beamformer	Optional and programmable

II. SYSTEM ARCHITECTURE

A. General Overview

Fig. 1 gives a high-level block diagram illustration of the multi-channel pre-beamformed DAQ system that we have developed, and its major specifications are listed in Table I. A photo of the physical appearance of the completed system is shown in Fig. 2. Note that our DAQ system is shaped by various design considerations; the key considerations are highlighted in the Appendix. During operation, the probe-connecting end of this system is plugged into one of the transducer ports on an Ultrasonix research system (Sonix-RP or SonixTOUCH Research), while an array probe performs scanning through another transducer port. Leveraging upon the fact all transducer ports on an Ultrasonix research system are wired in parallel, the DAQ system is capable of acquiring pre-beamformed raw data without disrupting the scanner's imaging operations, and in turn the scanner can be regarded as an image-guidance platform for pre-beamformed data acquisition. Synchronization between the DAQ system and the Ultrasonix scanner is achieved through two signals that are facilitated through two coaxial cable links. One of them, referred to as Sync in Fig. 1, is responsible for coordinating the start time of each pulse-echo firing event. The other, denoted Clock in Fig. 1, serves to unify the sampling clock signals on the two systems to avoid random jitters during pre-beamformed data capture resulting from clock phase misalignment.

Fig. 2. Photo of the multi-channel pre-beamformed data acquisition (DAQ) system. The four horizontally aligned boards at the bottom of the picture are the receiver boards (each responsible for DAQ over 32 channels); the one at the top is the main controller board. The left and right boards are, respectively, the power module and the connector board.

B. Description of System Operations

In general, the operations of our DAQ system can be considered as a cascade of processes that are distributed among various system components. At the beginning of a pulse-echo reception event, the transmit/receive (T/R) switches on the connector board (upper left side of Fig. 1) are responsible for activating the analog signal paths corresponding to the individual channels. The signals are then relayed to the analog-to-digital convertors (ADCs) on the four receiver boards (lower half of Fig. 1), each of which is responsible for performing 32 channels of time gain compensation (TGC), anti-alias filtering, amplification, and digitization. After that, the digitized signal samples of each transducer channel are de-serialized using hardware modules implemented in a field-programmable gate array (FPGA) and are stored into the DDR2 (double data rate, ver. 2) memory buffer (4 GB on each board, 16 GB total). As can be deduced from Eq. (1) in the Appendix, this memory is large enough to store pre-beamformed data samples of all 128 channels for 2 to 3 human cardiac cycles. Table II lists the system's DAQ capacity for four common imaging scenarios with different combinations of view depth and pulse repetition frequency (PRF). It can be seen that, in practical imaging settings, our DAQ system can capture raw data for at least 8000 transmit firings, corresponding to nearly a 2-s period. This is sufficient to facilitate experimental investigation of new imaging methods in commonly scanned areas of the body, such as carotid arteries, kidneys, heart, and the abdomen.

The main board of our DAQ system (upper right side of Fig. 1) is primarily in charge of controlling the T/R switches on the connector board, defining the TGC curves in the receiver boards, and coordinating the data retrieval process (as denoted by the cross-links between boards in Fig. 1). Implementation of these tasks is realized via an FPGA on the main board. If preferred, parts of the hardware resources on this FPGA and those on the receiver boards can also be reconfigured to perform on-board processing such as beamforming. Another purpose of the main board is to facilitate communication with a PC back-end through a USB 2.0 link. This is carried out via a data traffic controller implemented on the main-board FPGA. When the two devices are linked, the PC can program the FPGA on the main board, upload data acquisition parameters to the system's static random access memory (SRAM), and request that the DAQ system download pre-beamformed data samples. In our current implementation, the practical data transfer rate achievable with this USB link is around 20 MB/s. As such, complete download of the 16 GB pre-beamformed data buffer would require roughly 14 min. To help users perform these operations, a GUI has been developed using the Visual C++ language. A detailed description of each system component is provided in the next section.

III. System Components

A. Connector Board

As can be seen in Fig. 1, the connector board is one of the three major components in the pre-beamformed DAQ system that we have developed. A block diagram of how this board functions within our system is given in Fig. 3. Note that the board is connected to other system components (receiver boards and the main board) through analog and digital signal connectors. Its overall function is to interface the DAQ system with the array probe and the scanner, and its specific functions include:

TABLE II. Pre-Beamformed Data Acquisition (DAQ) Capacity for Common Ultrasound Imaging Scenarios (for 40 MHz Sampling Rate and 2 Bytes Per Sample).

	Carotid imaging	Abdominal imaging	Cardiac imaging	Renal imaging
Imaging depth (cm)	4	10	15	16
Nominal pulse repetition frequency (kHz)	10	6.6	5	3.3
DAQ capacity (no. of Tx firings supported)	25 830	12 917	8611	8073
Nominal DAQ duration* (s)	2.58	1.95	1.72	2.44

*DAQ duration can be varied by changing the PRF.

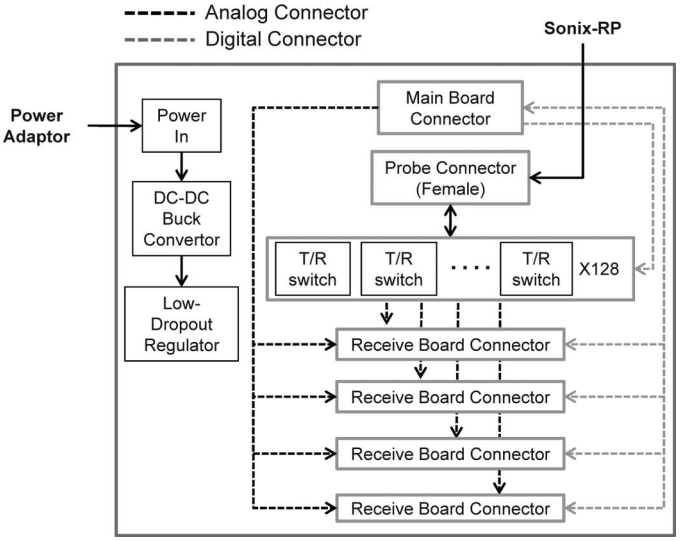

Fig. 3. Block diagram illustration of the connector board that serves as the interface between the data acquisition system, the array probe, and the scanner.

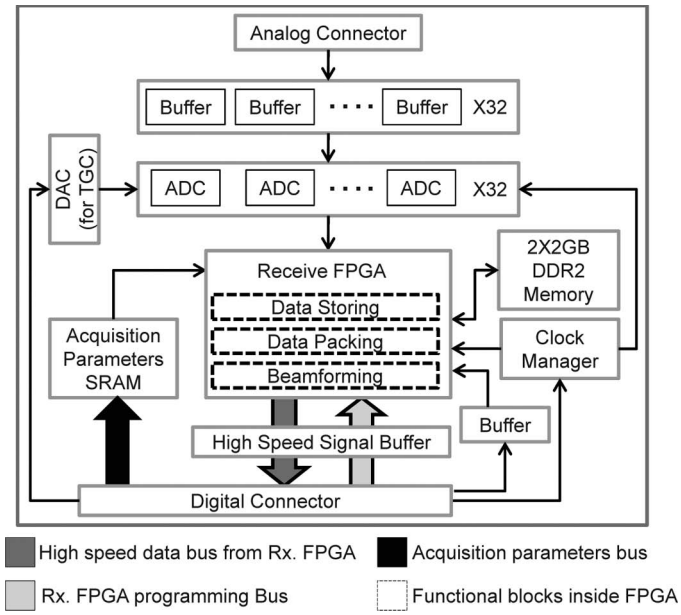

Fig. 4. Block diagram of the receiver board. Each board performs pre-beamformed data acquisition for 32 channels and stores the samples in a 4 GB RAM. It also amplifies, filters, and applies time gain compensation to the analog signals. Partial on-board beamforming can be carried out as well.

1) Interfacing with Scanner: A 156-pin Tyco male connector (Tyco Electronics Corporation, Berwyn, PA) is used as the probe connector on this board. It allows the DAQ system to be plugged into one of the probe ports on an Ultrasonix scanner, while the array transducer is connected to another probe connector. With such an arrangement, pulse-echo signals from the array probe can be passed into the DAQ system and the scanner in parallel (as discussed in Section II-A). This makes it possible for the scanner to perform image navigation without interruption while the DAQ system captures pre-beamformed data. It is worth noting that, because of this parallel configuration, the raw signals entering both the DAQ system and the Ultrasonix scanner inherently undergo a 3 dB signal decay as the signals are essentially shunted among these two systems.

2) T/R Switching: TX810 IC chips (Texas Instruments, Dallas, TX) are used to implement this functionality. Because our DAQ system is connected in parallel with the array transducer, the use of these switches is essential to isolate the DAQ electronics from the high-voltage electrical pulses that are sent into the array probe to drive the transducer elements. They are powered down on transmit to achieve electrical isolation, and on receive, they are switched on by injecting a bias current that is specified by the FPGA on the main board.

3) Supplying Power for System: Power is distributed through this board to the whole system. Various voltage inputs are supported to drive different system components.

B. Receiver Boards

Another key component in our pre-beamformed DAQ system is the set of four receiver boards that are individually responsible for acquiring 32 channels of digitized pre-beamformed data and storing them to the on-board DDR2 memory buffer. Fig. 4 gives an overview of how various blocks within the receiver board interact with each other. The specific functions of each receiver board include:

1) Applying TGC and Amplifying Signals: These are implemented using the built-in amplifiers within the ADCs used in our system (AD9272; Analog Devices, Norwood, MA). In particular, two stages of signal conditioning are performed within the ADCs. First, a set of low-noise amplifiers (LNAs), each with a maximum gain of 21.3 dB, is used to boost the incoming signals from each channel in parallel. After that, for each channel, TGC is applied as a signal attenuator with maximum attenuation down to −42 dB, and then further amplification is performed using a voltage-controlled amplifier (VCA) with a digitally tuneable gain between 21 and 30 dB. If no TGC is applied, an overall gain of 52 dB can be achieved in this system.

2) Filtering: The AD9272 ADCs have two built-in analog filters. The first is for anti-aliasing purposes before digital sampling; the second serves to suppress dc bias and flicker noise. The filter characteristics are adjustable within the ADCs.

3) Digital Sampling: After the amplification and filtering stages, the analog pulse echoes are digitized by the ADCs using one of two options: 1) 12-bit resolution for a 40-MHz sampling rate, or 2) 10-bit resolution for an 80-MHz sampling rate. Lower bit resolution for 80-MHz sampling is achieved in our DAQ system as a result of data rate constraints in the receiver-board FPGAs. To analyze

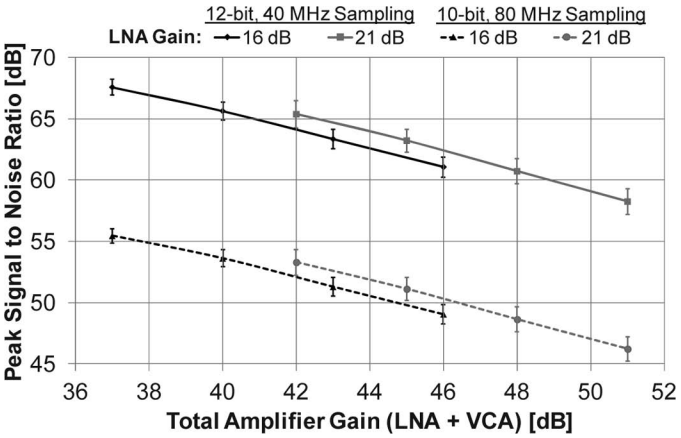

Fig. 5. Peak signal-to-noise ratio (PSNR) of pre-beamformed digitized samples for different amplification values (with no time gain compensation applied). Each line plots the PSNR for one particular low-noise amplifier (LNA) gain (16 or 21 dB) and four voltage-controlled amplifier (VCA) gain values (21, 24, 27, and 30 dB). Results are shown for both 12-bit, 40-MHz sampling (solid lines) and 10-bit, 80-MHz sampling (dashed lines). Error bars show PSNR standard deviation over 128 channels.

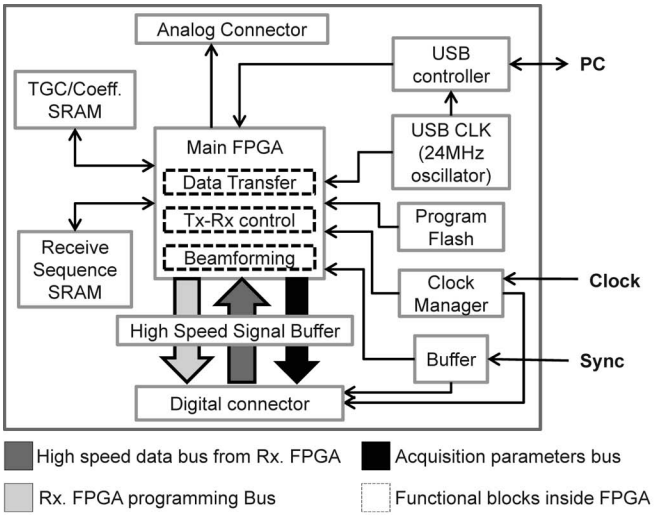

Fig. 6. Block diagram of the main board that acts as the controller for the data acquisition process from the array probe and the USB data transfer process. It also controls time gain compensation parameters and performs on-board beamforming.

the noise characteristics of the digitized samples, Fig. 5 shows the average pre-beamformed peak signal-to-noise ratio (PSNR) for various combinations of LNA and VCA gain values (without TGC attenuation). For each of the values shown, the noise level was measured experimentally by finding the average power of 2000 raw channel data (repeated over all 128 channels), which was acquired when the DAQ system was not connected to the scanner. It can be seen in Fig. 5 that, for 40-MHz sampling (with peak signed magnitude of $2^{11} = 2048$), the PSNR is between 58 and 68 dB (see solid lines) over the range of amplifier gains available in the ADC. For 80-MHz sampling (with peak signed magnitude of $2^9 = 512$), the PSNR is between 46 and 55 dB (see dashed lines). Note that the values reported in Fig. 5 are the expected PSNRs. It is clear that these values can only be achieved in the presence of strong reflectors. Note also that the PSNR is higher at lower gain levels because the noise floor increases as we increase the gain.

4) De-Serializing and Storing Data: These functions are facilitated by an on-board FPGA (Virtex-5 XC5VLX85; Xilinx Inc., San Jose, CA), where the digitized samples are fed into via low-voltage differential signaling (LVDS). In our system, two data samples are packed together to form a 32-bit data that is stored in the receiver board's 4 GB of DDR2 memory (16 GB total for the 4 receiver boards). We have empirically confirmed that, for 40-MHz sampling, the read/write speed of DDR2 memory is sufficient to handle the data traffic generated in the DAQ system. For 80-MHz sampling, an internal buffer has been implemented to cache 8000 samples before writing to the DDR2 memory.

5) Partial Beamforming and On-Board Processing (Optional): Parts of the hardware resources on the receiver-board FPGA may be reconfigured to perform partial beam summation over the 32 channels of pre-beamformed data to which each receiver board is assigned. This is meant to facilitate on-board implementation of novel beamforming strategies developed by imaging researchers. Each of these FPGAs has 48 digital signal processing (DSP) slices pre-allocated in the hardware, and they run at a 500 MHz clock rate, so the maximum computational power of each FPGA can reach 10^{10} floating point operations per second.

C. Main Board

In addition to the connector board and the receiver boards, the main board also plays an essential role in the DAQ system's operations. Fig. 6 shows the design of the main board's architecture in our DAQ system. This board is responsible for coordinating system components during data acquisition and managing data traffic with the PC back-end. It has the following specific functions:

1) Directing Signal Reception Events: This is implemented in the form of a T/R controller module within the Virtex-5 FPGA (Xilinx Inc.) on the main board. During operation, the controller first loads the receive parameters stored within the on-board SRAM (e.g., the enabled channel numbers, gain delay/offset, and receive delay). With these parameters, it then activates the corresponding T/R switches on the connector board upon receiving a trigger signal from the on-board Sync port (sent from the Ultrasonix scanner) that signifies the start of a pulse-echo firing event. This controller also synchronizes the digitization process over the 128 channels by instructing the FPGAs on the receiver boards to capture the signals once transmit signal is completed. These parameters can all be programmed via the USB 2.0 link.

2) Generating TGC Control Signals: This function is realized via a TGC controller that is implemented within the main-board FPGA. During operation, the controller first loads the TGC values either from the DAQ system's SRAM or from the host scanner depending on the user's choice. It then converts these values into analog TGC control signals via a digital-to-analog convertor (DAC) on the receiver boards. The analog signals are in turn sent to the ADCs on the receiver board to update the operating characteristics of their built-in VCAs.

3) Communicating with PC Back-End: A USB 2.0 controller (EZ-USB FX2; Cypress Semiconductor Corp., San Jose, CA) is installed on the main board to facilitate communication between the DAQ system and the PC back-end. It is mainly responsible for handling the transfer of data samples from the DAQ system's memory buffer to the PC. It also serves as a link for the PC to send programming bit-streams to the FPGAs on both the main board and receiver boards, as well as sending the pulse-sequencing parameters to the system's SRAM. In this work, we have connected the USB link to the Ultrasonix scanner's research platform, as it is based upon a PC architecture, and we have developed a GUI to facilitate user interactions with the DAQ system. It is also possible for the back-end to be a stand-alone PC that is not linked to the scanner.

4) Beamforming and On-Board Processing (Optional): If on-board beamforming is to be carried out, the main-board FPGA can serve as a controller that sends channel delay coefficients to the receiver-board FPGAs for partial beam summations over a subset of transducer channels. It can then serve as a hub that performs second-stage summation from the receiver boards' partially beamformed data to yield the final post-beamform data samples. With this two-stage beamforming architecture, users can have flexibility in exploring new beamforming algorithms that are not limited to delay-and-sum of adjacent transducer channels, as is typically done in B-mode imaging.

IV. Initial Performance Experiment

A. Efficacy in Pre-Beamformed Data Capture

To analyze the signal acquisition performance of our pre-beamformed DAQ system, we have performed an *in vitro* calibration experiment that involved cross-sectional imaging of a wire phantom. For this work, the Sonix-RP scanner was used as the host scanner for our DAQ system. A 128-element linear array probe (L14–5) was connected to the imaging platform, and it was dipped into a water bath with a 150-μm-diameter metal wire cross-section that was placed at 3.5 cm depth and was positioned at the probe center [see Fig. 7(a)]. Alignment was performed via the real-time image feedback available on the Sonix-RP scanner. The imaging parameters are summarized in Table III. Pre-beamformed pulse-echoes for each firing were captured and stored using our DAQ system.

Fig. 7(b) shows a plot of the pre-beamformed pulse echoes received from all 128 channels when the transmit aperture is at the probe center. The theoretical time-of-flight of the pulse echoes in each channel is also shown in this plot as a gray line. As can be seen, these pre-beamformed pulse echoes collectively resemble a parabolic pattern. This is consistent with theoretical predictions that stem from inter-element changes in the propagation distance [31], which in this case is the shortest for the center element and farthest at the edges.

B. Efficacy in Facilitating Studies of Beamforming Algorithms

Using the pre-beamformed data sets acquired over the wire target, we have investigated the efficacy of a few apodization strategies as applied to delay-and-sum beamforming. For this study, an in-house Matlab script (ver. 2010a; The MathWorks Inc., Natick, MA) was developed to perform dynamic receive beamforming from the pre-beamformed pulse echoes of each firing and, in turn, generate the RF signal for each beamline. Subsequently, B-mode images were produced using standard signal processing routines based on the beamformed RF signals. Note that the wire phantom was purposefully chosen to have a diameter of 150 μm so that the diameter is equal to the imaging wavelength in this study. Under such condition, the wire would not be simply visualized as a point target, and as a result of the inherent side lobes in the transmit beam, there may be significant artifacts that distort the image. Therefore, this imaging scenario serves as an efficacy test for whether a beamforming algorithm can facilitate sharp visualization of the wire.

Fig. 8 shows the resulting B-mode images generated from delay-and-sum beamforming for three different apodization windows: uniform, Hanning, and minimum-variance. The results are generally consistent with ultrasound beamforming theory that explains how non-uniform apodization may suppress spurious beam side lobes and, in turn, reduce reverberation artifacts [31]. The first two apodization windows are based on fixed coefficients and are commonly used in existing ultrasound scanners. Their resulting images [Figs. 8(a) and 8(b)] have apparent reverberation artifacts in the form of streaks and bands near the wire position at a depth of 3.5 cm. Comparing these two images, the Hanning window seems to provide a better visualization of the wire cross-section than the uniform window. In spite of this, further improvements in the wire cross-section's visualization have been demonstrated by the minimum-variance window [see Fig. 8(c)] that is based on adaptive computation of the apodization weights using the local signal statistics [21]. For this adaptive beamforming approach, its resulting image has fewer reverberation artifacts, likely because each pixel's magnitude is optimized to have minimum variance with respect

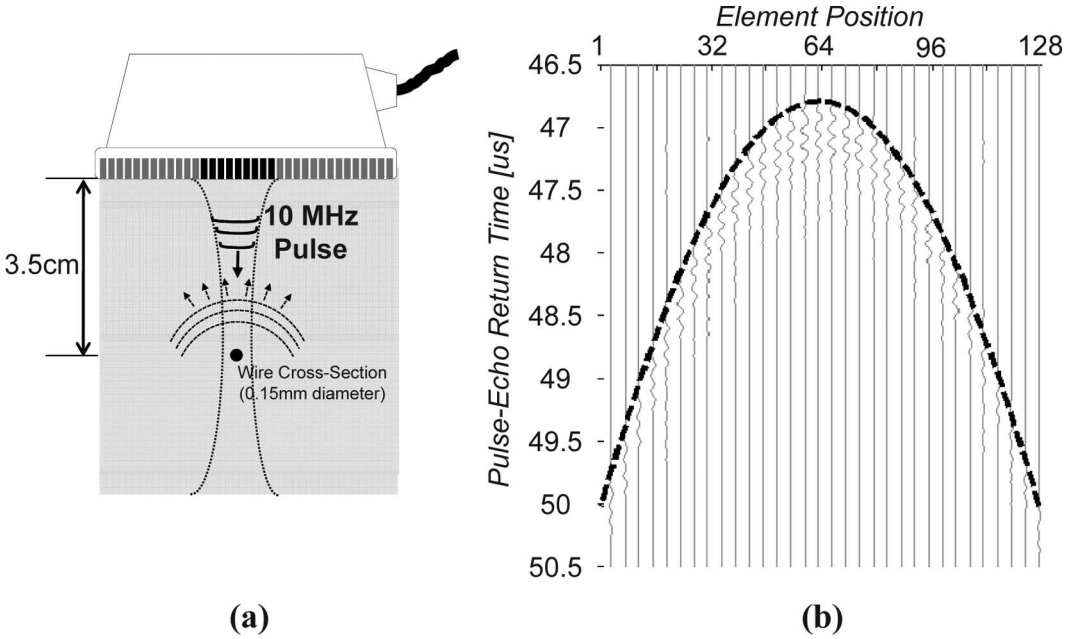

Fig. 7. Wire-phantom experiment for evaluating the pre-beamformed data acquisition performance of the developed system: (a) illustration of the imaging setup when the beamline is at the probe center; (b) the corresponding pre-beamformed pulse echoes acquired over the array channels in parallel (data shown over every four channels). The dashed line indicates the theoretical time-of-flight in each channel. Pulse echoes are normalized against the peak signal magnitude over all channels.

TABLE III. IMAGING PARAMETERS FOR THE CASE EXAMPLES.

Parameter	Wire imaging	B-flow imaging
Transmit aperture (no. of elements)	64	128
Receive aperture (no. of elements)	128	
Array pitch	0.3048 mm	
Amplifier gain	51 dB (no TGC applied)	
Transmit focusing depth (cm)	3.5	None
Pulse duration (μs)	0.2 (2 cycles)	0.6 (4 cycles)
Imaging frequency (MHz)	10	6.6
PRF (kHz)	N/A	2.5

TGC = time gain compensation; PRF = pulse repetition frequency.

to the focus-delayed channel-domain data samples for that pixel position.

V. CASE EXAMPLE OF PLANE-WAVE B-FLOW IMAGING

A. Experimental Procedure

As a case example of how our DAQ system can be used for advanced imaging investigations, an *in vitro* study was conducted to evaluate the efficacy of tracking blood speckles at high frame rates by combining plane-wave imaging principles [18] with the B-flow visualization technique [32], [33]. The imaging view of this pilot experiment is an in-plane slice of a commercially available Doppler calibration phantom (Model 1425A; Gammex Inc., Middleton, WI)

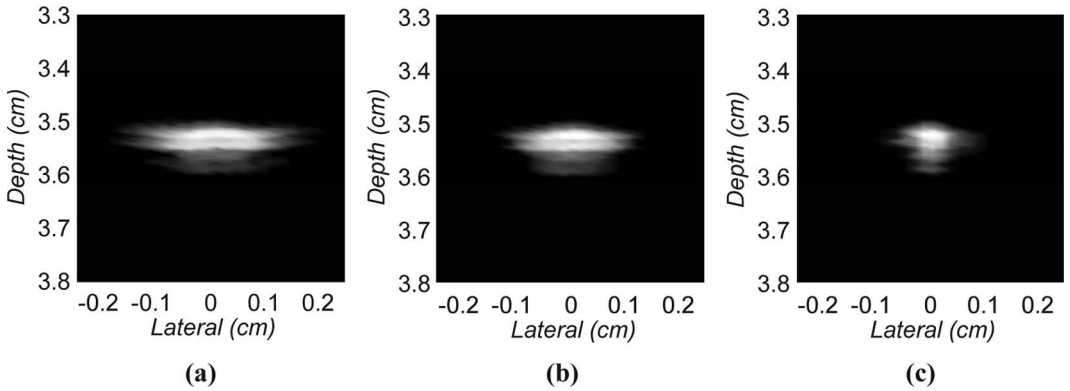

Fig. 8. B-mode images of a wire cross-section for different apodization windows: (a) uniform, (b) Hanning, (c) minimum variance. Images are obtained from processing pre-beamformed data acquired from the developed data acquisition system (128-channel delay-and-sum; 32-channel sub-apertures for minimum variance). Note that the wire diameter is the same as the imaging wavelength, so the cross-section is not being visualized as a point target.

with a 5-mm-diameter flow tube positioned at 3-cm depth with a 75° Doppler angle. During operation, the flow settings of the phantom were adjusted to generate a steady flow profile with a centerline velocity of 40 cm/s. Plane-wave imaging was performed on this *in vitro* configuration using a SonixTOUCH scanner whose transmit-firing sequence was redefined using the TEXO Software Development Kit (Ultrasonix). Specifically, unfocused plane-wave pulses were transmitted from the scanner's front-end by simultaneously exciting all 128 elements on an L9–4 linear array probe at a 2.5 kHz PRF (see Table III for other data acquisition parameters). On receive, our DAQ system was used to capture pre-beamformed pulse-echoes over all 128 array channels for 500 consecutive firings (i.e., 0.2 s total duration), after which they were transferred to a PC for offline processing.

B. Data Processing Procedure

To obtain plane-wave B-flow images, we have adopted a three-stage processing procedure. First, a plane-wave image was generated for each frame of pre-beamformed data by performing parallel receive beamforming (with dynamic focusing) via the use of an in-house Matlab script. In this study, 64 lateral lines spanning 1 cm were beamformed for each frame. In the second stage, blood speckles were computed in each plane-wave image by applying an inter-frame difference filter to each pixel. In the last stage, a B-flow image was synthesized for each frame by overlaying the respective blood speckles on top of the plane-wave image if their power was above a gain threshold. Cineloops were generated with multiple B-flow images to visualize the efficacy of tracking blood flow at high frame rates (in this case, at the 2.5 kHz PRF, or 2500 fps).

To facilitate comparison, we have computed conventional B-flow images by processing the pre-beamformed data using the B-mode imaging paradigm where at most a few lines are formed from each frame of pre-beamformed data. In this work, a quad-beam parallel receive beamformer was used to generate B-mode images over the same lateral span as the plane-wave images. As such, the frame rate of the resulting cineloops effectively was reduced by a factor of 16 (down to 156 fps).

C. Imaging Results and Discussion

Fig. 9 shows a representative frame of B-flow image obtained using plane-wave imaging and quad-beam B-mode imaging. Their corresponding cineloops have been included as multimedia attachments (). In the cineloops, the B-flow images were played back at slow motion without dropping frames (96 and 6 fps for plane-wave imaging and quad-beam imaging, respectively). This was done to better visualize the temporal resolving power of each imaging paradigm in depicting flow motion. The key observation to be noted is that the high temporal resolution offered by plane-wave imaging has enabled smooth visualization of the laminar flow inside the tube (see cineloop). In particular, it is evident from the blood speckles in the cineloop that the centerline flow is traversing the field-of-view at a faster speed than the flow near the tube wall. This cannot be clearly visualized in the quad-beam B-flow images, as its temporal resolution is not sufficient to track the fast-moving blood speckles (at 40 cm/s centerline velocity, the inter-frame displacement is 0.26 cm for a 156 fps frame rate—i.e., one-quarter of the lateral image span).

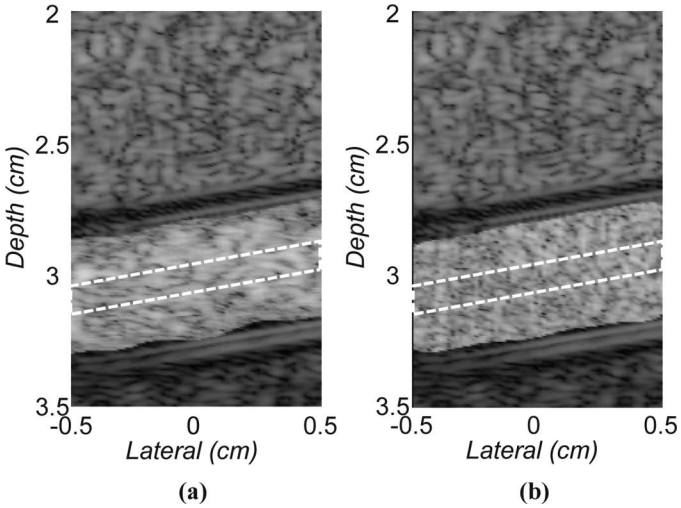

Fig. 9. Representaive B-flow image frames of a 5-mm-diameter steady-flow phantom positioned at 3 cm depth and at 75° Doppler angle. Results are shown for two paradigms: (a) plane-wave imaging ; (b) quad-beam B-mode imaging . See the cineloops for visualization performance over time. The dashed polygon indicates the region where the interframe correlation coefficient is estimated.

Another observation to be noted from Fig. 9 and its cineloop () is that the blood speckle pattern appeared to be more laterally coherent in plane-wave B-flow images compared with the quad-beam B-flow image frames. This is likely attributed to plane-wave imaging's ability to simultaneously acquire blood signals from the entire field-of-view with a single transmit firing. On the other hand, because conventional beamline-based imaging acquires blood signals in the field-of-view using multiple firings, blood scatterers are likely to have moved during the data acquisition process, and thus the resulting blood speckle pattern in the B-flow images would be less laterally coherent.

As a quantitative insight into the flow visualization quality, Fig. 10 shows the inter-frame correlation coefficient of the blood speckles within a 1-mm centerline window labeled in Fig. 9. It is evident that plane-wave B-flow imaging maintains a high correlation between adjacent frames (near 0.9), and thus a good visualization performance of blood speckles can be expected. In contrast, conventional B-flow imaging had a low inter-frame correlation coefficient in this example (at best around 0.4). This explains why the blood speckle pattern appeared to be incoherent between frames for this approach. Note that if focused transmit beams are used

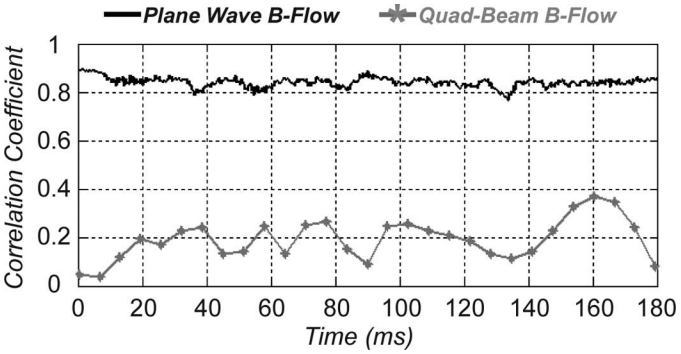

Fig. 10. Interframe correlation coefficient of blood speckles over the window labeled in Fig. 9. Results are shown for both plane-wave and quad-beam B-flow imaging. Fewer measurements are available for quad-beam B-flow imaging given its lower frame rate.

for beamline-based imaging, the inter-frame correlation coefficient would likely be further reduced because, between firings for the same lateral position, it becomes more probable for blood scatterers to move out of the transmit beam zone.

VI. Conclusion

This work set out to provide ultrasound imaging researchers with access to pre-beamformed ultrasound data required to pursue experimental evaluation of next-generation ultrasound imaging paradigms. The DAQ system developed by our team should be of strategic importance to many ultrasound imaging researchers, because it can enable them to pursue advanced imaging research projects that are no longer limited to simulations and computational analyses. It is our hope that our developed system can attract more ultrasound researchers to engage in imaging projects and in turn develop various novel imaging methods that can potentially offer higher frame rates and improved image quality. With the enriched research efforts and the expedited development pace in this area, it is likely that ultrasound imaging will further establish itself as a real-time, non-invasive imaging modality that can provide accurate visualization of anatomical structures and physiological functioning.

Appendix
Summary of System Design Considerations

There are two tiers of technical considerations that we have taken into account during the development process for our DAQ system. The first relates to the high-level design factors that shape the overall system structure; the second is pertinent to the choice of hardware components for our system. Details on each tier of design considerations are discussed in the following subsections.

A. Considerations for System Architecture

1) Plug-and-Play Functionality: One of the primary factors that shaped our design is the ability for our system to operate as a plug-and-play device. Specifically, it is our intent to connect our DAQ system to an Ultrasonix research scanner while the scanner operates as usual. This allows the user to concurrently perform diagnostic scans and capture pre-beamformed data, thereby exploiting the scanner essentially as a navigation platform for the DAQ system (the scanner would be operating in research mode under such a configuration). In our design, we have realized this feature by interfacing the DAQ system with an Ultrasonix scanner through one of the scanner's probe ports while the transducer array is connected to another.

2) Parallel Data Acquisition Capability: For our system to support research on advanced ultrasound imaging methods such as synthetic aperture imaging, it must be capable of collecting pre-beamformed data simultaneously from a large number of transducer array elements. Taking into account this consideration, we have made use of 16 octal-channel ADCs (AD9272; Analog Devices Inc.) in our system to acquire pre-beamformed data from 128 transducer array elements in parallel.

3) System Reconfigurability: Another major consideration that we have accounted for is the system's flexibility in reconfiguring data acquisition sequences and parameters as well as implementing on-board processing. This is an essential feature for research-oriented users who are interested in exploring new imaging paradigms. As such, we have included the use of high-end FPGAs (Virtex 5; Xilinx Inc.) in our DAQ system. Users may use our developed hardware modules on the FPGAs to facilitate coordination of data acquisition processes based on sequences and parameters that are loaded onto the system's SRAM, or they may program their own FPGA modules to implement new data acquisition strategies and beamforming algorithms.

B. Considerations for Choice of System Components

1) Sampling Rate: In typical imaging applications, the ultrasound frequency is usually below 20 MHz. Hence, according to the Nyquist theorem, the sampling frequency should be at least 40 MHz to prevent aliasing. The sampling rate should also be sufficiently high so as to reduce the error caused by applying the delay during beamforming. In this work, the AD9272 ADCs that we chose have a maximum sampling rate of 80 MHz.

2) Bit Resolution: Because of issues such as attenuation, the dynamic range for the received signal can be quite large over depth even after amplification and TGC. As such, digitization of analog signals should be done at a high bit resolution so that the imaging depth will not be severely limited. The AD9272 ADCs chosen for our system have been configured to operate in two modes: 12-bit sampling at 40 MHz and 10-bit sampling at 80 MHz. Note that 12-bit sampling at 80 MHz is technically achievable with AD9272, but this was not implemented in our system

because of transfer rate limitations in the receive-board FPGA.

3) Memory Size: Parallel data acquisition inherently leads to a large data throughput. In addition, in some clinical studies such as cardiac imaging, pre-beamformed data over a few consecutive seconds would be needed to properly assess the efficacy of new ultrasound imaging algorithms. Hence, a large memory buffer is needed to store all the acquired data before downloading to the PC back-end. It can be readily shown that the buffer size needed per imaging frame, in bytes, is equal to the following expression for a given maximum imaging depth ($d_{\max}$), acoustic speed (c_o), sampling rate (f_S), number of transmit firings (N_T), number of receive channels (N_R), and number of bytes needed for each sample (N_B):

$$N_{\text{buffer}} = N_T \cdot N_R \cdot N_B \cdot (2d_{\max}/c_o) \cdot f_S. \qquad (1)$$

In our system, we chose to include 16 GB of DDR2 memory as the storage buffer, whose size is sufficient to meet the DAQ requirements in practical imaging scenarios as summarized in Table II.

Acknowledgment

We are grateful to thank P. Y. S. Cheung (University of Hong Kong) for his enthusiastic support and encouragement on this work.

References

[1] P. N. T. Wells, "Ultrasound imaging," *Phys. Med. Biol.*, vol. 51, no. 13, pp. R83–R98, 2006.

[2] C. Basoglu, R. Managuli, G. York, and Y. Kim, "Computing requirements of modern medical diagnostic ultrasound machines," *Parallel Comput.*, vol. 24, no. 9–10, pp. 1407–1431, 1998.

[3] National Cancer Institute "Ultrasonic imaging: Infrastructure for improved imaging methods," in *Report of the OWH/NCI Sponsored Workshop*, 1999.

[4] P. Tortoli and J. A. Jensen, "Introduction to the special issue on novel equipment for ultrasound research," *IEEE Trans. Ultrason. Ferroelectr. Freq. Control*, vol. 53, no. 10, pp. 1705–1706, 2006.

[5] M. Ashfaq, S. S. Brunke, J. J. Dahl, H. Ermert, C. Hansen, and M. F. Insana, "An ultrasound research interface for a clinical system," *IEEE Trans. Ultrason. Ferroelectr. Freq. Control*, vol. 53, no. 10, pp. 1759–1771, 2006.

[6] V. Shamdasani, U. Bae, S. Sikdar, Y. M. Yoo, K. Karadayi, R. Managuli, and Y. Kim, "Research interface on a programmable ultrasound scanner," *Ultrasonics*, vol. 48, no. 3, pp. 159–168, 2008.

[7] L. Y. L. Mo, D. DeBusschere, W. Bai, D. Napolitano, A. Irish, S. Marschall, G. W. McLaughlin, Z. Yang, P. L. Carson, and J. B. Fowlkes, "Compact ultrasound scanner with built-in raw data acquisition capabilities," in *Proc. IEEE Ultrason. Symp.*, 2007, pp. 2259–2262.

[8] L. Masotti, E. Biagi, M. Scabia, A. Acquafresca, R. Facchini, A. Ricci, and D. Bini, "FEMMINA real-time, radio-frequency echo-signal equipment for testing novel investigation methods," *IEEE Trans. Ultrason. Ferroelectr. Freq. Control*, vol. 53, no. 10, pp. 1783–1795, 2006.

[9] S. Ricci, E. Boni, F. Guidi, T. Morganti, and P. Tortoli, "A programmable real-time system for development and test of new ultrasound investigation methods," *IEEE Trans. Ultrason. Ferroelectr. Freq. Control*, vol. 53, no. 10, pp. 1813–1819, 2006.

[10] H. J. Hewener, H. J. Welsch, C. Gunther, H. Fonfara, S. H. Tretbar, and R. M. Lemor, "A highly customizable ultrasound research platform for clinical use with a software architecture for 2D-/3D-reconstruction and processing including closed-loop control," in *Proc. Int. Fed. Med. Biol. Eng.*, 2009, pp. 342–345.

[11] T. Wilson, J. Zagzebski, T. Varghese, Q. Chen, and M. Rao, "The Ultrasonix 500RP: A commercial ultrasound research interface," *IEEE Trans. Ultrason. Ferroelectr. Freq. Control*, vol. 53, no. 10, pp. 1772–1782, 2006.

[12] K. Dickie, C. Leung, R. Zahiri, and L. Pelissier, "A flexible research interface for collecting clinical ultrasound images," *Proc. SPIE*, vol. 7494, art. no. 749402, 2009.

[13] T. H. Marwick, "Measurement of strain and strain rate by echocardiography," *J. Am. Coll. Cardiol.*, vol. 47, no. 7, pp. 1313–1327, 2006.

[14] S. Bjærum, H. Torp, and K. Kristoffersen, "Clutter filters adapted to tissue motion in ultrasound color flow imaging," *IEEE Trans. Ultrason. Ferroelectr. Freq. Control*, vol. 49, no. 6, pp. 693–704, 2002.

[15] A. C. H. Yu and L. Lovstakken, "Eigen-based clutter filter design for ultrasound color flow imaging: A review," *IEEE Trans. Ultrason. Ferroelectr. Freq. Control*, vol. 57, no. 5, pp. 1096–1111, 2010.

[16] L. Sandrin, S. Catheline, M. Tanter, X. Hennequin, and M. Fink, "Time-resolved pulsed elastography with ultrafast ultrasonic imaging," *Ultrason. Imaging*, vol. 21, no. 4, pp. 259–272, 1999.

[17] J. A. Jensen, S. I. Nikolov, K. L. Gammelmark, and M. H. Pedersen, "Synthetic aperture ultrasound imaging," *Ultrasonics*, vol. 44, suppl. 1, pp. e5–e15, 2006.

[18] G. Montaldo, M. Tanter, J. Bercoff, N. Benech, and M. Fink, "Coherent plane-wave compounding for very high frame rate ultrasonography and transient elastography," *IEEE Trans. Ultrason. Ferroelectr. Freq. Control*, vol. 56, no. 3, pp. 489–506, 2009.

[19] L. Sandrin, S. Manneville, and M. Fink, "Ultrafast two-dimensional ultrasonic speckle velocimetry: A tool in flow imaging," *Appl. Phys.*, vol. 78, no. 8, pp. 1155–1158, 2001.

[20] J. Udesen, F. Gran, K. L. Hansen, J. A. Jensen, C. Thomsen, and M. B. Nielsen, "High frame-rate blood vector velocity imaging using plane waves: Simulations and preliminary experiments," *IEEE Trans. Ultrason. Ferroelectr. Freq. Control*, vol. 55, no. 8, pp. 1729–1743, 2008.

[21] J. F. Synnevåg, A. Austeng, and S. Holm, "Adaptive beamforming applied to medical ultrasound imaging," *IEEE Trans. Ultrason. Ferroelectr. Freq. Control*, vol. 54, no. 8, pp. 1606–1613, 2007.

[22] C. Li and L. V. Wang, "Photoacoustic tomography and sensing in biomedicine," *Phys. Med. Biol.*, vol. 54, no. 19, pp. R59–R97, 2009.

[23] C. M. Fabian, K. N. Ballu, J. A. Hossack, T. N. Blalock, and W. F. Walker, "Development of a parallel acquisition system for ultrasound research," in *Proc. SPIE Med. Imag.*, 2001, pp. 54–62.

[24] L. Mo, D. DeBusschere, G. McLaughlin, D. Napolitano, W. Bai, K. Fowkees, A. Irish, X. Wang, J. B. Fowlkes, and P. L. Carson, "Compact ultrasound scanner with simultaneous parallel channel data acquisition capabilities," in *Proc. IEEE Ultrason. Symp.*, 2008, pp. 1342–1345.

[25] R. Diagle, "Ultrasound imaging system with pixel oriented processing," WIPO Patent Applicat. WO/2006/113445.

[26] L. Sandrin, M. Tanter, S. Catheline, and M. Fink, "Shear modulus imaging using 2D transient elastography," *IEEE Trans. Ultrason. Ferroelectr. Freq. Control*, vol. 49, no. 4, pp. 426–435, 2002.

[27] J. A. Jensen, O. Holm, L. J. Jensen, H. Bendsen, S. I. Nikolov, B. G. Tomov, P. Munk, M. Hansen, K. Salomonsen, J. Hansen, K. Gormsen, H. M. Pedersen, and K. L. Gammelmark, "Ultrasound research scanner for real-time synthetic aperture data acquisition," *IEEE Trans. Ultrason. Ferroelectr. Freq. Control*, vol. 52, no. 5, pp. 881–891, 2005.

[28] J. A. Jensen, M. Hansen, B. G. Tomov, S. I. Nikolov, and H. Holten-Lund, "System architecture of an experimental synthetic aperture real-time ultrasound system," in *Proc. IEEE Ultrason. Symp.*, 2007, pp. 636–640.

[29] P. Tortoli, L. Bassi, E. Boni, A. Dallai, F. Guidi, and S. Ricci, "ULA-OP: An advanced open platform for ultrasound research," *IEEE Trans. Ultrason. Ferroelectr. Freq. Control*, vol. 56, no. 10, pp. 2207–2216, 2009.

[30] J. L. Lu, J. Cheng, and J. Wang, "High frame rate imaging system for limited diffraction array beam imaging with square-wave aperture weightings," *IEEE Trans. Ultrason. Ferroelectr. Freq. Control*, vol. 53, no. 10, pp. 1796–1812, 2006.

[31] R. S. C. Cobbold, *Foundations of Biomedical Ultrasound*. New York, NY: Oxford University Press, 2007.
[32] R. Y. Chiao, L. Y. Mo, A. L. Hall, S. C. Miller, and K. E. Thomenius, "B-mode blood flow (B-flow) imaging," in *Proc. IEEE Ultrason. Symp.*, 2000, pp. 1469–1472.
[33] L. Lovstakken, S. Bjaerum, D. Martens, and H. Torp, "Blood flow imaging—A new real-time, 2-D flow imaging technique," *IEEE Trans. Ultrason. Ferroelectr. Freq. Control*, vol. 53, no. 2, pp. 289–299, 2006.

Chris C. P. Cheung received the B.S.E.E. degree in electrical and computer engineering from the University of Wisconsin–Madison in 1996. Since 1999, he has been working in the ultrasound industry. He is now an Ultrasound Hardware Engineering Manager in the Research and Development department of the Ultrasonix Medical Corporation, Richmond, Canada. Throughout his career, he has been involved in developing five successful medical ultrasound platforms, including the Sonix-RP system, which is widely used by medical ultrasound researchers.

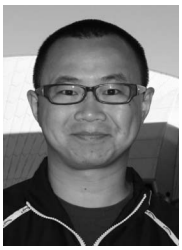

Alfred C. H. Yu (S'99–M'07) was born in Hong Kong in 1980. He is now a Research Assistant Professor in the Medical Engineering Program and the Department of Electrical and Electronic Engineering at the University of Hong Kong. He obtained his undergraduate degree in electrical engineering from the University of Calgary, AB, Canada, in 2002. He then completed his M.A.Sc. degree and Ph.D. training in biomedical engineering at the University of Toronto, ON, Canada, in 2003 and 2006, respectively. In between, he also completed a corporate internship at Philips Research North America, Briarcliff Manor, NY, in 2005. His current research interest focuses on three areas of biomedical ultrasound: development of new system hardware, design of novel imaging paradigms, and cellular investigations of ultrasound-induced therapeutic effects.

Nazila Salimi received her B.Sc. degree in electrical engineering from the University of Tehran. Her first M.Sc. degree in computer engineering (hardware engineering) was completed at the Amirkabir University of Technology. She obtained her second M.Sc. degree in geomatics engineering at the University of Calgary, and then joined the Research and Development department of the Ultrasonix Medical Corporation in 2007. Her research interest includes signal processing and real-time processing.

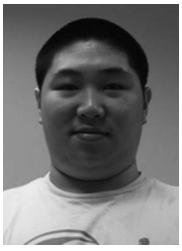

Billy Y. S. Yiu (M'10) was born and raised in Hong Kong. He is now working as a Research Engineer in the Biomedical Ultrasound Laboratory at the University of Hong Kong. He obtained his B.Eng.(Hons) degree in medical engineering in 2007, and completed the M.Phil. degree in electrical and electronic engineering in 2010, both at the University of Hong Kong. His current research interest is in ultrasound imaging, specifically in the development of imaging methods and systems.

Ivan K. H. Tsang completed his B.Eng.(Hons) degree in medical engineering at the University of Hong Kong in 2007, and finished his M.Phil. degree in electrical and electronic engineering from the same university in 2010. His thesis research was on designing ultrasound system hardware and developing novel imaging methods. He is now pursuing a teaching career in the Hong Kong secondary school system.

Benjamin Kerby received the B.Sc. degree in mathematics from Trinity Western University in 2003 and the B.A.Sc. degree in electrical engineering from the University of British Columbia in 2008. He has worked in software development at Ultrasonix Medical Corporation since 2008 and is now the Software Team Lead.

Reza Zahiri Azar (S'05–M'10) received the B.Sc. degree in computer engineering from Sharif University of Technology in 2003, the M.A.Sc. degree in electrical and computer engineering from the University of British Columbia (UBC) in 2005, and the Ph.D. degree in electrical engineering from UBC in 2009. He is recipient of the David W. Strangway Fellowship and NSERC Industrial Research and Development Fellowship. He is currently a Research Scientist at the Research and Development department of the Ultrasonix Medical Corporation, Richmond, Canada. He is also a Research Associate at the ECE department of the UBC. His research interests mainly include motion estimation, flow estimation, and tissue characterization and modeling for medical applications and diagnosis.

Kris Dickie joined Ultrasonix Medical Corporation in 2000 as a software engineer, where he quickly became acquainted with ultrasound technology and the field of medical research. Today, he manages the research and OEM business of Ultrasonix, which includes almost 200 installations of university-based research devices and other start-ups making use of Ultrasonix OpenSONIX technology. Kris holds a B.Tech degree in computer systems from the British Columbia Institute of Technology, Burnaby, Canada.